





Characterizing coastal phytoplankton seasonal succession patterns on the West Antarctic Peninsula

Schuyler C. Nardelli ^{1,*} Patrick C. Gray ² Sharon E. Stammerjohn ³ Oscar Schofield ¹

¹Rutgers University Center for Ocean Observing Leadership, Rutgers University, New Brunswick, New Jersey

²Duke University Marine Lab, Duke University, Beaufort, North Carolina

³Institute of Arctic and Alpine Research, University of Colorado, Boulder, Colorado

Abstract

In coastal West Antarctic Peninsula (WAP) waters, large phytoplankton blooms in late austral spring fuel a highly productive marine ecosystem. However, WAP atmospheric and oceanic temperatures are rising, winter sea ice extent and duration are decreasing, and summer phytoplankton biomass in the northern WAP has decreased and shifted toward smaller cells. To better understand these relationships, an Imaging FlowCytobot was used to characterize seasonal (spring to autumn) phytoplankton community composition and cell size during a low (2017–2018) and high (2018–2019) chlorophyll *a* year in relation to physical drivers (e.g., sea ice and meteoric water) at Palmer Station, Antarctica. A shorter sea ice season with early rapid retreat resulted in low phytoplankton biomass with a low proportion of diatoms (2017–2018), while a longer sea ice season with late protracted retreat resulted in the opposite (2018–2019). Despite these differences, phytoplankton seasonal succession was similar in both years: (1) a large-celled centric diatom bloom during spring sea ice retreat; (2) a peak summer phase comprised of mixotrophic cryptophytes with increases in light and postbloom organic matter; and (3) a late summer phase comprised of small (< 20 μm) diatoms and mixed flagellates with increases in wind-driven nutrient resuspension. In addition, cell diameter decreased from November to April with increases in meteoric water in both years. The tight coupling between sea ice, meltwater, and phytoplankton species composition suggests that continued warming in the WAP will affect phytoplankton seasonal dynamics, and subsequently seasonal food web dynamics.

Coastal waters along the West Antarctic Peninsula (WAP) host a highly productive, ice-dependent marine ecosystem fueled by large, seasonal phytoplankton blooms reaching chlorophyll *a* (Chl *a*) concentrations > 20 mg m^{-3} (Vernet et al. 2008; Ducklow et al. 2013; Kim et al. 2018). Average primary productivity in the WAP is $\sim 182 \text{ g C m}^{-2} \text{ yr}^{-1}$, which is similar to other continental shelf areas in Antarctica (Arrigo et al. 2008), but four times lower than other productive coastal regions in the world's oceans (Vernet and Smith 2007).

*Correspondence: scn50@scarletmail.rutgers.edu

This is an open access article under the terms of the [Creative Commons Attribution-NonCommercial](#) License, which permits use, distribution and reproduction in any medium, provided the original work is properly cited and is not used for commercial purposes.

Additional Supporting Information may be found in the online version of this article.

Author Contribution Statement: S.N. and O.S. designed the study and analysis. S.N. and S.S. acquired data. S.N., S.S., and P.G. performed data analysis. S.N. prepared figures and drafted the original manuscript. S.N., P.G., S.S., and O.S. helped with interpretation of data and edited the manuscript.

Phytoplankton blooms along the WAP initiate in the austral spring when increased solar irradiance alleviates light limitation, and sea ice melt stratifies the upper water column and confines phytoplankton in well-lit surface waters (Vernet et al. 2008; Venables et al. 2013). Macronutrients and micronutrients are generally replete in coastal WAP waters (Kim et al. 2016; Sherrell et al. 2018; Carvalho et al. 2020), thus upper water column stratification is considered the primary driver of phytoplankton productivity (Garibotti et al. 2005a; Vernet et al. 2008; Carvalho et al. 2020). Interannual phytoplankton dynamics are tightly coupled to krill recruitment (Saba et al. 2014), and krill in turn are the main food source for penguins, seals, whales, and other predators (Ducklow et al. 2013), suggesting a strong bottom-up control of the ecosystem. Thus, studying how coastal phytoplankton communities respond to physical drivers is imperative for understanding ecosystem structure and function.

The coastal WAP phytoplankton community is comprised of diatoms, cryptophytes, mixed flagellates, prasinophytes, and haptophytes, with diatoms making up the highest percentage of annual biomass (Varela et al. 2002; Garibotti et al. 2005a; Schofield et al. 2017). However, different

phytoplankton species require specific abiotic conditions for optimal growth, causing both seasonal and interannual variability in community composition. Earlier studies have tried to reconstruct seasonal succession at Palmer Station; however, validation of these hypotheses is still an open question as the results are either based on phytoplankton accessory pigments only capable of resolving general taxa (Schofield et al. 2017), or do not span a full austral spring to autumn range (Garibotti et al. 2005a). In general, these studies found three successional phases in the coastal WAP: (1) a diatom-dominated bloom comprised primarily of large centric diatoms associated with spring sea ice retreat and upper water column stratification in November/December, (2) a cryptophyte-dominated community associated with low Chl *a*, decreased nutrient stocks, and shallow mixed layer depths in December/January, and (3) a diatom-enriched assemblage associated with low Chl *a* including small diatoms, haptophytes, and unidentified flagellates in February/March.

Significant environmental change is impacting the productive WAP ecosystem. One of the fastest warming regions on Earth, WAP winter air temperatures and surface ocean temperatures have increased by $> 6^{\circ}\text{C}$ and $> 1^{\circ}\text{C}$, respectively, since 1951 (Meredith and King 2005; Turner et al. 2005). In response, 90% of marine glaciers were in retreat as of 2016, the annual sea ice season has decreased by > 92 d since 1979, and there is no longer perennial sea ice in the northern WAP (Stammerjohn et al. 2012; Cook et al. 2016). Ocean warming, sea ice and glacial retreat, and glacial melt have in turn impacted the phytoplankton community, with significant decreases in January mean phytoplankton biomass along the northern WAP corresponding with a shift from large ($> 20\ \mu\text{m}$) to small-celled ($< 20\ \mu\text{m}$) phytoplankton (Montes-Hugo et al. 2009). It is hypothesized that this size shift is driven by increasing cryptophyte (cell diameters of $\sim 6.5\text{--}9\ \mu\text{m}$) abundance in coastal regions that are often associated with low salinity meltwater (Moline et al. 2004; Mendes et al. 2013; Schofield et al. 2017). The reasons why cryptophytes might outcompete diatoms in low-salinity waters are not well understood, but are hypothesized to be related to an advanced light-adaptation system that allows them to thrive in stratified surface waters with high irradiances (Kaña et al. 2012; Mendes et al. 2018a). The increased spatial extent of low salinity surface waters is predicted to increase the prevalence of smaller-celled phytoplankton communities along the WAP (Moline et al. 2004), with important implications for food web structure and trophic energy transfer efficiency (Sailley et al. 2013).

The Palmer Long-Term Ecological Research Project (PAL-LTER) was established in 1991 to investigate how warming and sea ice loss will change the structure of the pelagic ecosystem and biogeochemistry along the WAP. The project has previously used high-performance liquid chromatography (HPLC) analysis of pigment data to characterize the taxonomic composition of phytoplankton assemblages (e.g., Schofield et al. 2017).

This technique uses marker pigments of phytoplankton groups to assess their contributions to overall abundance. Few studies have looked at higher taxonomic resolution and cell size distributions over seasonal scales along the WAP.

Our study utilized an imaging-in-flow cytometer to characterize seasonal and interannual phytoplankton diversity at Palmer Station, Antarctica, with a focus on local sea ice and meltwater impacts. We sampled both a high and low Chl *a* year to investigate (1) interannual differences in the physical environment and corresponding differences in phytoplankton communities, and (2) potential mechanisms driving phytoplankton seasonal succession. Results showed that despite significant differences in sea ice dynamics and phytoplankton biomass between years, there were consistent seasonal succession patterns. In addition, environmental disturbances (e.g., spring sea ice retreat, upper water column mixing, glacial melt, and sea ice melt) throughout the growing season drove changes in phytoplankton community composition that could not be described using HPLC alone. These findings provide insights into regulation of WAP seasonal phytoplankton dynamics and help hypothesize how ongoing warming and melting might impact future coastal phytoplankton communities.

Methods

Sample collection

Annual sample collection at Palmer Station, Antarctica (Fig. 1) has been conducted by the PAL-LTER since 1991 at two locations: an inshore station (Sta. B, bottom depth of ~ 75 m) and an offshore station (Sta. E, bottom depth of ~ 200 m). These stations are sampled twice per week from approximately early November (when the sea ice cover breaks up) to late March. Inclement weather and heavy sea ice can impede sampling in this region, leading to occasional gaps in the dataset. Our study focused on two austral summer field seasons: 2017–2018 (16 November–26 March), which had lower than average Chl *a* and was preceded by a shorter than average winter sea ice duration, and 2018–2019 (02 November–28 March), which had higher than average Chl *a* and was preceded by a longer than average winter sea ice duration (Fig. S1). Because we were interested in the impacts of sea ice and glacial meltwater on inshore phytoplankton communities, our analysis exclusively used surface samples from Sta. B, which is adjacent to the Marr Ice Piedmont (Fig. 1). For each sampling event, a SeaBird Electronics Seacat SBE 19plus sensor (measuring salinity, temperature, and depth) was profiled down to 60 m. These data were averaged into 1-m depth bins. In addition, surface seawater samples were collected with a 4 L Niskin bottle and stored in a cold, dark environment until sample processing at Palmer Station.

Phytoplankton pigment analysis

Concentrations of Chl *a* and accessory pigments were measured via HPLC. Whole seawater (1–2 L) was filtered onto GF/F

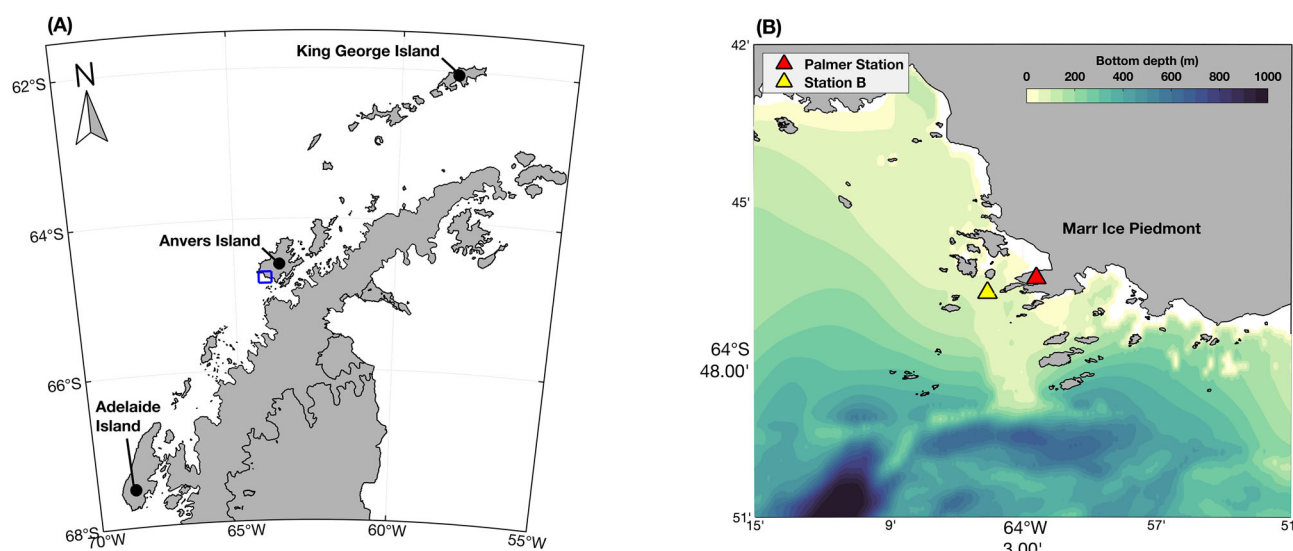


Fig. 1. (A) Map of the West Antarctic Peninsula with the blue box indicating the extents of the Palmer region shown in (B).

filters (pore size = $0.7 \mu\text{m}$, diameter = 25 mm), flash-frozen in liquid nitrogen, and stored at -80°C for analysis after the field season. The samples were shipped to Rutgers University (New Brunswick, NJ), where they were run on the HPLC system following methods in Carvalho et al. (2020). Using the output HPLC pigment data, phytoplankton taxonomic composition was quantitatively determined in CHEMTAX V1.95 using pigment ratios derived from WAP phytoplankton (Kozłowski et al. 2011). Output phytoplankton groups include diatoms, cryptophytes, prasinophytes, haptophytes, and mixed flagellates (including both dinoflagellates and other phytoflagellates). Although there are alternative methods to quantify Antarctic Peninsula phytoplankton taxonomic groups from CHEMTAX data (e.g., Mendes et al. 2018b), we used methods from Kozłowski et al. (2011) to remain consistent with previously published datasets from the PAL-LTER.

Phytoplankton species and cell size analysis

For species identification and cell size distributions, 5 mL of each surface sample was analyzed with an Imaging FlowCytobot (IFCB; McLane Labs). The IFCB is an imaging-inflow cytometer that uses a combination of imaging and flow cytometric technology to collect images and measure Chl *a* fluorescence and scattered light for each particle (~ 10 – $150 \mu\text{m}$) in each water sample (Olson and Sosik 2007). Samples were passed through a $150 \mu\text{m}$ Nitex screen prior to analysis to prevent large cells from clogging the IFCB's flow cell. Cells with major axis length < 20 pixels ($5.88 \mu\text{m}$) were eliminated from the analysis as the resolution of the images was insufficient to provide clear identification.

Images were extracted from IFCB files and processed using methods and software from Sosik and Olson (2007) (<https://github.com/hsosik/ifcb-analysis/wiki>). Image processing creates a set of 233 features describing each image including

equivalent spherical diameter, area, and biovolume of each cell. Processed images were then sorted into 40 taxonomic groups using a medium complexity convolutional neural network ($\sim 2,000,000$ parameters) that was created and validated using WAP phytoplankton (Nardelli et al. 2022). Processed images, along with their predicted identifications, associated features, and metadata were uploaded to the web application EcoTaxa (Picheral et al. 2017; <https://ecotaxa.obs-vlfr.fr>), where predicted images were manually validated.

Identification of individual cells was performed to the highest possible taxonomic resolution given image resolution, for example, most diatoms were identified to genus/species level and most phytoflagellates were identified to class level (cryptophyte, haptophyte, and prasinophyte; see Table 1), with guidance from Hasle et al. (1997) and Scott and Marchant (2005). Mixed flagellates included dinoflagellates (e.g., *Gymnodinium* spp., *Gyrodinium* spp., and others), silicoflagellates (e.g., *Dictyochaetes* spp.), and other unidentified phytoflagellates. Prasinophytes primarily included *Pyramimonas* spp. and *Pterosperma* spp., and haptophytes primarily included *Phaeocystis antarctica*. Diatoms were divided into centric and pennate groups (see Table 1). Unidentified centric discoid cells included *Thalassiosira* spp., *Coscinodiscus* spp., *Minidiscus chilensis*, *Porosira* spp., *Actinocyclus actinochilus*, *Asteromphalus hookeri*, and *Stellarima microtrias*, among others. Unidentified pennate cells included *Banquisia belgicae*, *Membraneis* spp., *Navicula* spp., *Fragilariopsis* spp., and *Nitzschia* spp., among others. Chains of unidentified centric and pennate diatom species were included in the $> 20 \mu\text{m}$ category.

In addition, aggregated metrics for all phytoplankton cells and for the six broad taxonomic groups (centric diatoms, pennate diatoms, cryptophytes, mixed flagellates, haptophytes, and prasinophytes) were calculated for each sample. These

Table 1. Median phytoplankton cell size (μm) for each taxonomic group in each successional phase using IFCB data.

Taxonomic groups	Spring ice retreat		Peak summer		Late summer	
	<i>n</i>	Median \pm std	<i>n</i>	Median \pm std	<i>n</i>	Median \pm std
Cryptophytes	9133	8.51 \pm 1.18	10,723	8.67 \pm 1.46	2305	8.67 \pm 1.71
Mixed flagellates	18,993	5.81 \pm 2.38	18,933	5.61 \pm 2.05	29,944	5.63 \pm 1.73
Haptophytes	5695	6.75 \pm 1.99	2253	5.68 \pm 0.75	3273	5.69 \pm 0.77
Prasinophytes	3148	8.40 \pm 1.52	1180	7.97 \pm 1.21	991	8.36 \pm 2.61
Diatoms	24,164	5.94 \pm 5.32	31,301	5.75 \pm 1.97	20,075	6.19 \pm 3.79
Centric diatoms	7026	7.07 \pm 8.86	3097	7.85 \pm 4.05	5061	12.89 \pm 4.42
<i>Chaetoceros</i> spp.	545	6.30 \pm 9.81	26	9.77 \pm 6.56	88	14.67 \pm 9.45
<i>Corethron pennatum</i>	97	31.08 \pm 18.76	0	NA	12	38.81 \pm 12.15
<i>Eucampia antarctica</i>	29	43.18 \pm 14.90	1	84.45	1	44.05
<i>Dactyliosolen</i> spp.	9	13.16 \pm 10.76	0	NA	3	8.77 \pm 1.16
<i>Odontella weissflogii</i>	1	53.29	0	NA	0	NA
<i>Proboscia</i> spp.	7	47.14 \pm 19.13	3	45.47 \pm 14.60	2	45.94 \pm 13.26
Unidentified 0–10 μm	4835	6.90 \pm 0.83	2033	6.97 \pm 1.05	1388	7.13 \pm 0.97
Unidentified 10–15 μm	716	12.15 \pm 1.31	858	12.53 \pm 1.35	2609	13.22 \pm 1.19
Unidentified 15–20 μm	217	16.06 \pm 1.21	150	16.06 \pm 1.11	874	15.91 \pm 1.03
Unidentified > 20 μm	570	39.87 \pm 20.92	26	27.72 \pm 9.96	84	29.77 \pm 9.43
Pennate diatoms	17,138	5.57 \pm 2.58	28,204	5.67 \pm 1.12	15,014	5.81 \pm 1.97
<i>Amphiprora</i> spp.	46	16.98 \pm 4.51	0	NA	0	NA
<i>Cocconeis</i> spp.	4	14.25 \pm 3.45	13	12.05 \pm 7.47	25	12.84 \pm 3.83
<i>Cylindrotheca</i> spp.	228	9.81 \pm 2.14	1	10.84	6	9.06 \pm 0.75
<i>Licmophora</i> spp.	7	16.15 \pm 6.46	16	15.49 \pm 4.73	19	14.56 \pm 6.86
<i>Pseudo-nitzschia</i> spp. chains	371	14.73 \pm 3.74	15	12.03 \pm 2.71	113	14.12 \pm 4.21
Unidentified 0–10 μm	15,987	5.51 \pm 0.92	27,955	5.66 \pm 0.72	14,227	5.75 \pm 1.12
Unidentified 10–15 μm	352	11.17 \pm 1.20	168	11.08 \pm 1.14	573	10.97 \pm 1.13
Unidentified 15–20 μm	58	17.72 \pm 1.41	13	16.34 \pm 1.52	34	17.45 \pm 1.47
Unidentified > 20 μm	85	24.77 \pm 6.64	23	24.88 \pm 5.04	17	25.03 \pm 5.27

include total biovolume (sum biovolume of all cells in a sample divided by the mL of water sampled), total abundance (total number of cells in a sample divided by the mL of water sampled), and median cell diameter.

Since IFCB-derived phytoplankton biovolume and HPLC-derived Chl *a* concentrations were both estimates of total phytoplankton biomass for each method, we compared the two using Kendall rank correlation to confirm general agreement. To validate taxonomic precision, IFCB data were separated into broad taxonomic groups matching those derived from HPLC (diatoms, cryptophytes, prasinophytes, haptophytes, mixed flagellates). Then, the methods were compared for each taxonomic group by evaluating the Kendall rank correlation between percent taxa in each sample for both methods.

In both years, preserved samples (5 mL whole seawater in 50% glutaraldehyde) were collected during times when the IFCB was not available (i.e., undergoing maintenance or aboard the vessel on the annual 1-month WAP cruise). Fixed samples were flash-frozen in liquid nitrogen and stored at -80°C for analysis after the field season. In 2017–2018, samples were preserved from 05 January to 05 February, and

in 2018–2019, samples were preserved on 13 December and from 07 January to 28 March. On 22, 26, and 28 December 2017, live samples were collected alongside preserved samples for comparison. On average, total biovolume and cell abundance of preserved samples were underestimated by 48.07% and 36.36%, respectively, when compared to live samples (Fig. S2A,B). However, relative changes in biovolume and abundance were similar between the three samples (Fig. S2A,B), as were the relative percentages of different taxonomic groups (Fig. S2C–E). Cryptophytes and prasinophytes were consistently found at higher percentages in preserved vs. live samples, indicating a potential preservation bias toward these groups (on average 17.38% more cryptophytes and 32.86% more prasinophytes in preserved samples; Fig. S2C–E).

To quantify phytoplankton diversity from IFCB data, the Shannon diversity index (*H*) was used, which describes the number and richness of groups sampled:

$$H = - \sum_{i=1}^R p_i \ln p_i,$$

where p_i is the proportion of individuals in the i th group identified in the dataset and R is the total number of groups identified in the data set. Higher values of H suggest that there are both more groups represented in the data set and more members of each of those groups. An H value of zero indicates only one group present in the dataset.

Ancillary data

Sea ice metrics were calculated from satellite-derived daily sea ice concentration (%) data determined using the GSFC Bootstrap algorithm version 3.1 and extracted for the 25 km \times 25 km satellite pixel closest to Palmer Station. Following methods in Stammerjohn et al. (2008), day of ice-edge advance was calculated as the first day when sea ice concentration exceeded a 15% threshold for at least 5 consecutive days; day of ice-edge retreat was calculated as the last day before sea ice concentration dropped below a 15% threshold after being above 15% for at least 5 consecutive days; sea ice duration is the number of days between the day of advance and the day of retreat, and number of sea ice days are the number of days between the day of advance and day of retreat where sea ice concentration is $> 15\%$.

Meltwater composition was derived from oxygen isotope composition ($\delta^{18}\text{O}$) once per week. Water from each surface sample was drawn into a 50 mL glass vial, sealed with a stopper and aluminum crimp, and stored in a dark, $+4^\circ\text{C}$ box. Samples were transported to the National Environmental Isotope Facility at the British Geological Survey (Keyworth, Nottinghamshire, UK). There, an Isoprime 100 mass spectrometer plus Aquaprep device were used to analyze $\delta^{18}\text{O}$ using the CO_2 equilibration method. Measurements were calibrated against internal and international standards (e.g., VSMOW2 and VSLAP2). An analytical reproducibility of $\pm 0.02\text{‰}$ was obtained with duplicate analysis. Using $\delta^{18}\text{O}$ and surface salinity data, we quantitatively separated sea ice melt from meteoric water (glacial melt, precipitation, and runoff from snow melt) by solving a three-endmember mass balance equation (see methods and endmember values in Meredith et al. 2021). Using this mass balance equation, negative values for sea ice melt are possible and are indicative of net sea ice formation (i.e., more sea ice grew in situ than melted in situ due to lateral advection). Glacial meltwater discharge is a dominant meteoric source in the coastal and nearshore regions of the WAP (Meredith et al. 2013, 2017, 2021), but here we will continue to refer to this derived metric as “meteoric water” to explicitly reflect the fact that it comprises both precipitation and glacial meltwater inputs.

Surface samples were analyzed for nitrate plus nitrite ($\text{NO}_3^- + \text{NO}_2^-$; hereafter called nitrate due to the very low concentration of nitrite), phosphate (PO_4^{3-}), and silicate ($\text{Si}[\text{OH}]_4^-$). Each surface sample (1 L) was filtered through GF/F filters (pore size = $0.7 \mu\text{m}$, diameter = 25 mm) and stored at -20°C in 15 mL acid-rinsed Falcon centrifuge tubes. The samples were shipped to Lamont Doherty Earth Observatory

at Columbia University (New York, NY), where they were analyzed following methods in Carvalho et al. (2020).

Mixed layer depths could not be confidently predicted ($\text{QI} < 0.5$; Lorbacher et al. 2006) at Sta. B due to the shallow water depth (~ 60 m). Thus, mean Brunt–Väisälä frequency (N^2) values were calculated for the top 25 m using methods from Carvalho et al. (2017) to quantify and compare upper water-column stability within and between our two sampling years.

Wind speed (m s^{-1} ; RM Young, Model 05108-45) and photosynthetically active radiation (PAR; $\mu\text{mol s}^{-1} \text{m}^{-2}$; Licor, Model LI 190) measurements were obtained from an automated weather station located just behind Palmer Station. Five-day means of wind speed (current day and the four previous days) and daily mean PAR were calculated from 2-min data.

Statistical analyses

One-way analysis of variances with Kruskal–Wallis post hoc tests were conducted for each environmental variable (sea ice concentration, PAR, surface temperature, surface salinity, percent meteoric water, percent sea ice meltwater, N^2 , wind speed, nitrate, phosphate, and silicate) and phytoplankton variable (Chl a concentration, H , and IFCB-derived phytoplankton biovolume, abundance, and median diameter), to determine whether values were significantly different between the two field seasons.

To assess relationships between environmental and phytoplankton variables, we conducted a principal components analysis (PCA) on all data from both years, using z-scores from environmental (sea ice concentration, PAR, surface temperature, surface salinity, percent meteoric water, percent sea ice meltwater, N^2 , wind speed, nitrate, and silicate) and phytoplankton (percent biovolume attributed to centric diatoms, pennate diatoms, cryptophytes, mixed flagellates, prasinophytes, and haptophytes) variables. Linear interpolation was used to fill in missing values in the environmental data—this included 7 values in the nitrate and silicate data, and 39 values in the percent meteoric water and sea ice melt data over both seasons ($\delta^{18}\text{O}$ was only sampled once per week). Using a k -means cluster analysis on the same dataset, a silhouette test identified three clusters representing successional phases: a Spring Ice Retreat Phase, a Peak Summer Phase, and a Late Summer Phase. Kendall rank correlation tests were used to quantify relationships found in the PCA. Nonparametric statistics were used due to the non-normal data distributions for most variables.

Results

HPLC vs. IFCB taxonomy comparison

HPLC-derived Chl a concentrations were significantly positively correlated to IFCB-derived biovolume concentrations (Fig. S3). The two methods yielded similar timing and magnitude of biomass peaks within each field season, with notable

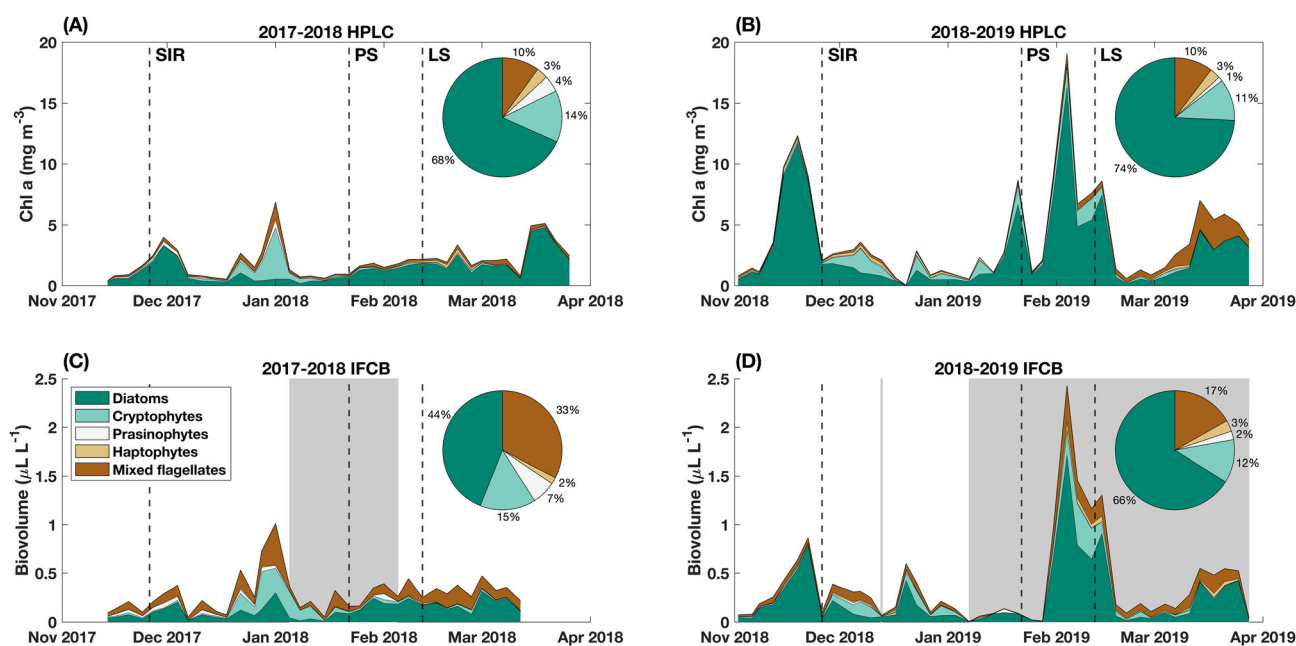


Fig. 2. Spring to autumn (A and B) HPLC-derived chlorophyll *a* and (C and D) IFCB-derived biovolume for each phytoplankton group. Pie chart insets show total percent (A and B) chlorophyll *a* or (C and D) biovolume for each group over the entire field season. Gray areas in plots C and D indicate periods when IFCB results are based on preserved samples. Vertical dashed lines indicate the overall mean date of each seasonal succession phase (SIR = Spring Ice Retreat Phase, PS = Peak Summer Phase, and LS = Late Summer Phase).

differences including much lower relative peaks for IFCB-derived biovolume on 19 November 2018 and 21 January 2019 compared to HPLC-derived Chl *a* (Fig. 2).

In addition, there were significant, positive correlations between percent taxa calculated with each method for diatoms, cryptophytes, prasinophytes, and mixed flagellates (Fig. S4A–D), and a nonsignificant, positive correlation for haptophytes (Fig. S4E). However, IFCB classification over-predicted mixed flagellates compared to HPLC classification, illustrated by the skew of points above the 1 : 1 line in Fig. S4D, and by the greater total percent of mixed flagellates classified by the IFCB than by HPLC for the entire field season (23% greater in 2017–2018 and 7% greater in 2018–2019; Fig. 2). Similarly, IFCB classification under-predicted diatoms compared to HPLC classification, illustrated by the skew of points below the 1 : 1 line in Fig. S4A, and by the lesser total percent of diatoms classified by the IFCB than by HPLC for the entire field season (24% lesser in 2017–2018 and 8% lesser in 2018–2019; Fig. 2). Despite discrepancies between methods, IFCB data provided information that HPLC data could not, including cell size and species composition within taxonomic groups (Table 1).

Interannual differences

Compared to the winter of 2018, the winter of 2017 had a later fall sea ice-edge advance date (17 July 2017 vs. 01 July 2018), an earlier spring sea ice-edge retreat date (02 December 2017 vs. 26 December 2018), shorter sea ice season duration

(138 d in 2017 vs. 178 d in 2018), and less total sea ice days (125 d in 2017 vs. 177 d in 2018; Fig. 3A,B). Sea ice was rapidly advected from the region in 2017, dropping from 49% on 27 November to 0% on 03 December (Fig. 3A). In 2018, there was an initial drop in sea ice concentration from 96% on 02 November to 29% on 05 November, but sea ice remained steady at an average of 34.8% until it retreated on 26 December, with intermittent advection in and out of the region until 16 January (Fig. 3B).

Consistent with rapid advection, there were no positive sea ice melt contributions to coastal surface waters in 2017 (Fig. 3C), while there were significant positive contributions in November and December in 2018 (Fig. 3D). $\delta^{18}\text{O}$ -derived freshwater sources (sea ice melt and meteoric water) reflect the net seasonal freshwater balance, so negative values of percent sea ice melt indicate that seasonally, there was net sea ice growth in the Palmer region (i.e., more sea ice grew here than melted here). Thus, negative values in November and December 2017 likely indicate that sea ice was grown in the Palmer region the previous autumn–winter and melted elsewhere in spring, whereas positive values in December and January 2018 indicate local spring melting that exceeds the previous autumn–winter local growth. During the sampling period (01 November–31 March), sea ice concentrations were significantly higher in 2018–2019 than in 2017–2018 (Table S1). Aside from interannual differences in sea ice due to wind-driven advection, the physical and biogeochemical environments were relatively similar between the 2 yr, except for

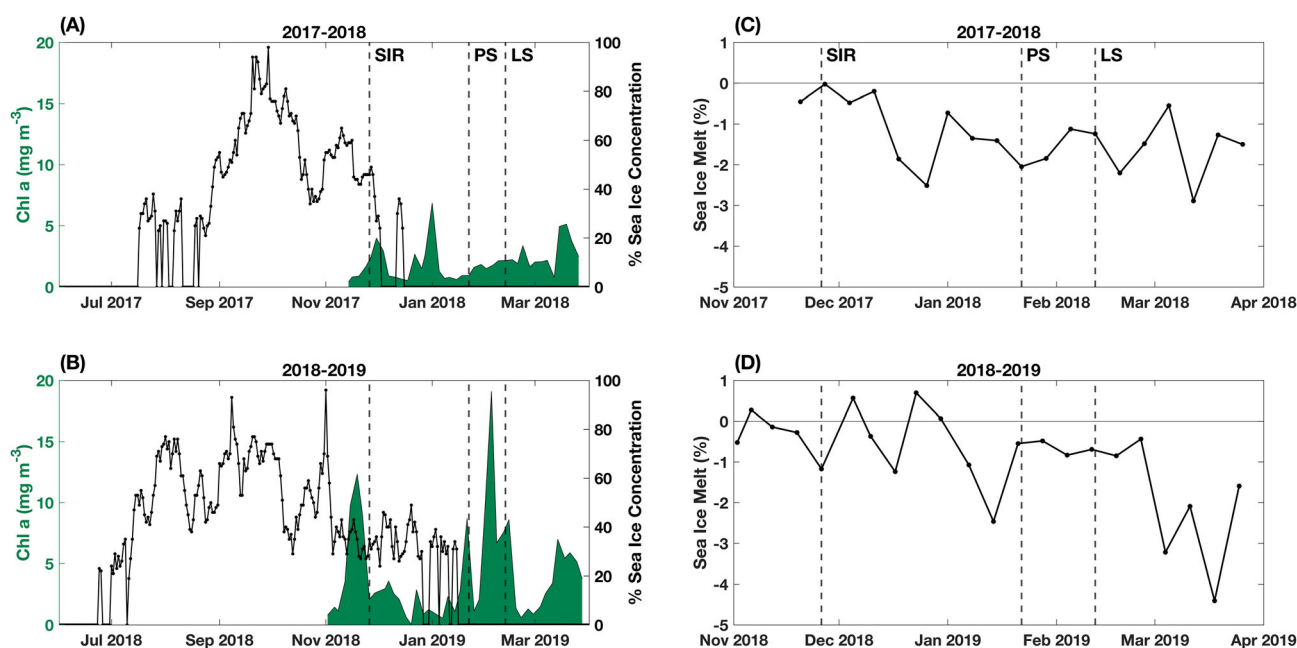


Fig. 3. Spring to autumn (A and B) chlorophyll *a* concentration (green) overlaid with daily percent sea ice concentration (black line) for (A) 2017–2018 and (B) 2018–2019. Percent sea ice melt for (C) 2017–2018 and (D) 2018–2019, where positive values indicate net seasonal sea ice melt and negative values indicate net seasonal sea ice formation. Vertical dashed lines indicate the overall mean date of each seasonal succession phase (SIR = Spring Ice Retreat Phase, PS = Peak Summer Phase, and LS = Late Summer Phase).

higher temperatures in 2017–2018, and higher concentrations of nitrate and silicate in 2018–2019 (Table S1).

Phytoplankton data showed significantly higher Chl *a* concentrations in 2018–2019, but significantly lower *H* values indicating fewer species and less evenness in species abundance (Table S2). Taxonomically, there were greater percent diatom and haptophyte biovolumes in 2018–2019, and greater percent mixed flagellate and prasinophyte biovolumes in 2017–2018 (Fig. 2 pie charts; Table S3).

Spring–autumn successional trends

PCA results showed seasonal changes in the environment that were reflected in phytoplankton successional changes averaged over both field seasons (Fig. 4). The three calculated clusters occurred sequentially in time, with cluster 1 (Spring Ice Retreat Phase) centered at 26 November, cluster 2 (Peak Summer Phase) centered at 22 January, and cluster 3 (Late Summer Phase) centered at 12 February (Fig. 4; Table S5). See Figs. S5–S8 for the full timeseries of each dataset.

Compared to the other two phases, the Spring Ice Retreat Phase was characterized by relatively high sea ice concentrations (mean = 39%) and sea ice melt (mean = -0.3%), high wind speeds (mean = 6.1 m s^{-1}) and corresponding lower water column stability (mean = 9.2×10^{-5}), high nutrient concentrations (mean nitrate = $23.5 \mu\text{mol L}^{-1}$, mean phosphate = $1.7 \mu\text{mol L}^{-1}$, and mean silicate = $67.1 \mu\text{mol L}^{-1}$), cold surface water temperatures (mean = -0.7°C) and high surface water salinities (mean = 33.5 ppt; Fig. 5; Table S5). As sea ice concentrations dropped below $\sim 50\%$ in November, the first bloom of the

season occurred. This Spring Ice Retreat Phase bloom contained the highest diversity of the season (Fig. 5O) and was comprised of high centric diatom abundance (55% of total biovolume), and comparatively high seasonal prasinophyte (5% total biovolume, mainly *Pyramimonas* spp.) and haptophyte abundances (3% total biovolume, mainly *P. antarctica*; Fig. 6A; Table 1). These centric diatoms were 78% unidentified discoid cells with diameters $> 20 \mu\text{m}$, likely consisting of a mix of large, chain-forming diatoms including *Thalassiosira* spp. (Fig. 6B). Centric diatom species including *Chaetoceros* spp., *C. pennatum*, and *Eucampia antarctica*, and pennate diatom species including *Amphiprora* spp., *Cylindrotheca* spp., and *Pseudo-nitzschia* spp. chains had their highest cell counts during this phase (Table 1).

The Peak Summer Phase was a transition phase characterized by relatively high surface temperatures (mean = 1.0°C) and surface salinities (mean = 33.5 ppt), low wind speeds (mean = 4.3 m s^{-1}) and moderate water column stability (mean = 1.2×10^{-4}), less sea ice melt (mean = -0.9%) but higher meteoric water percentages (mean = 4.2%), lower nutrient concentrations (mean nitrate = $21.1 \mu\text{mol L}^{-1}$, mean phosphate = $1.6 \mu\text{mol L}^{-1}$, and mean silicate = $67.0 \mu\text{mol L}^{-1}$), and high but variable PAR (mean = $399.7 \mu\text{m s}^{-1} \text{ m}^{-1}$; Fig. 5; Table S5). Sea ice concentrations were negligible during this phase (mean = 1.8%; Fig. 5D; Table S5). The Peak Summer Phase had the lowest Chl *a* concentrations but highest IFCB-derived biovolume and abundance values, and the lowest phytoplankton diversity of the season (Fig. 5K–M,O). The Peak Summer Phase was associated with high cryptophyte abundance (29% total biovolume), mixed flagellate abundance (27%

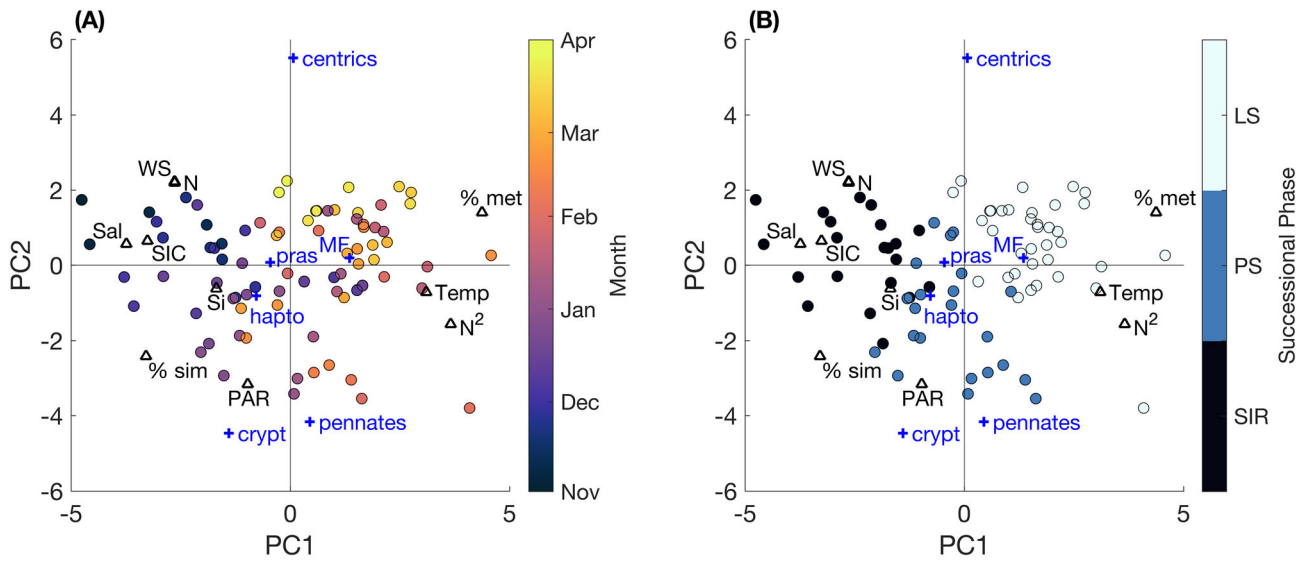


Fig. 4. PCA results showing loadings: triangles for environmental variables (Temp = temperature, Sal = salinity, WS = wind speed, SIC = sea ice concentration, % sim = % sea ice melt, % met = % meteoric water, N = nitrate, and Si = silicate) and + for phytoplankton variables (centrics = centric diatoms, pennates = pennate diatoms, crypt = cryptophytes, MF = mixed flagellates, pras = prasinophytes, and hapto = haptophytes), with values multiplied by 10 for readability; and circles represent the coordinate for each sample based on the magnitude of PC1 and PC2 and in (A) are color coded by date, and in (B) are color coded by the three successional phases determined by *k*-means clustering (SIR = Spring Ice Retreat Phase, PS = Peak Summer Phase, LS = Late Summer Phase). The first two principal components represent 24.5% variance and 14.16% variance, respectively.

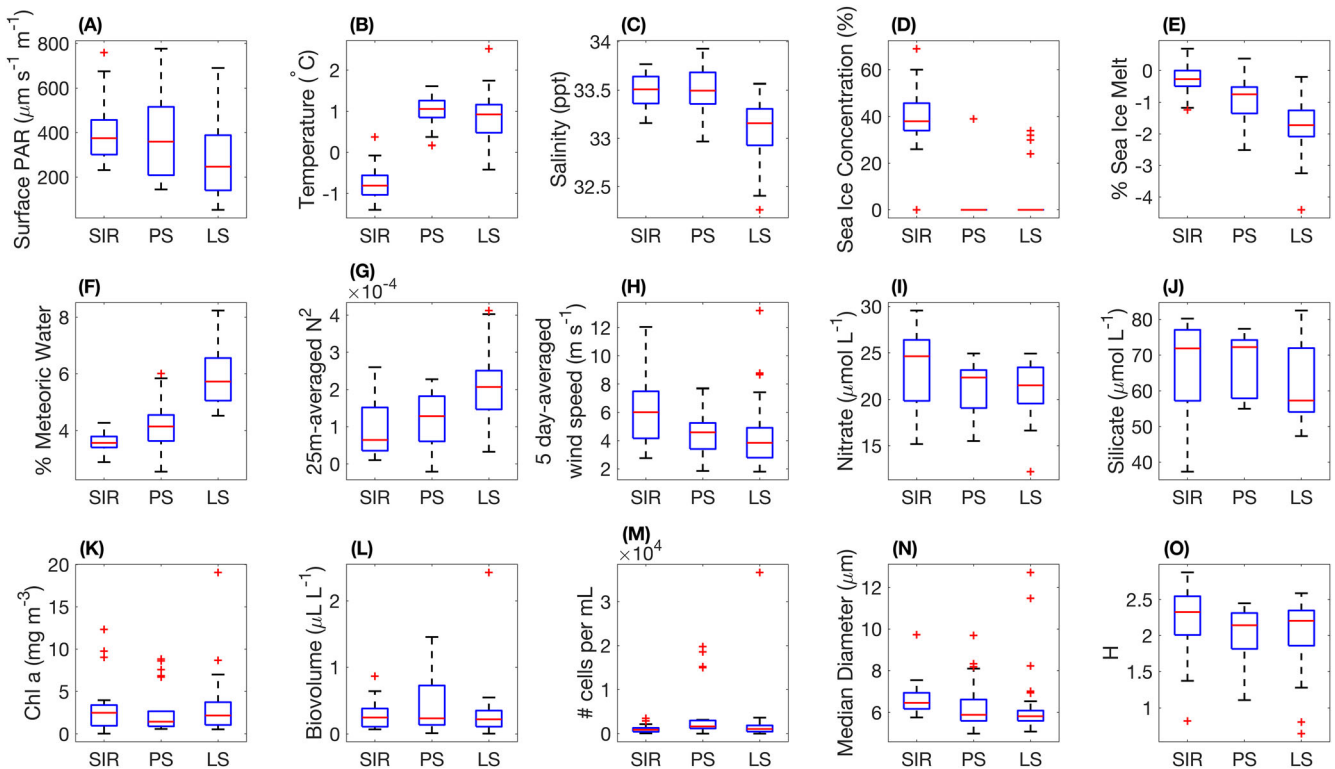


Fig. 5. Boxplots showing aggregated (A–J) environmental and (K–O) phytoplankton data over the 2 yr for the three successional phases: Spring Ice Retreat Phase (SIR), Peak Summer Phase (PS), and Late Summer Phase (LS). In each box plot, the horizontal red line represents the median value, the top and bottom box limits represent the 25th and 75th percentiles, whiskers represent the full range of non-outlier observations, and red + symbols represent outliers.

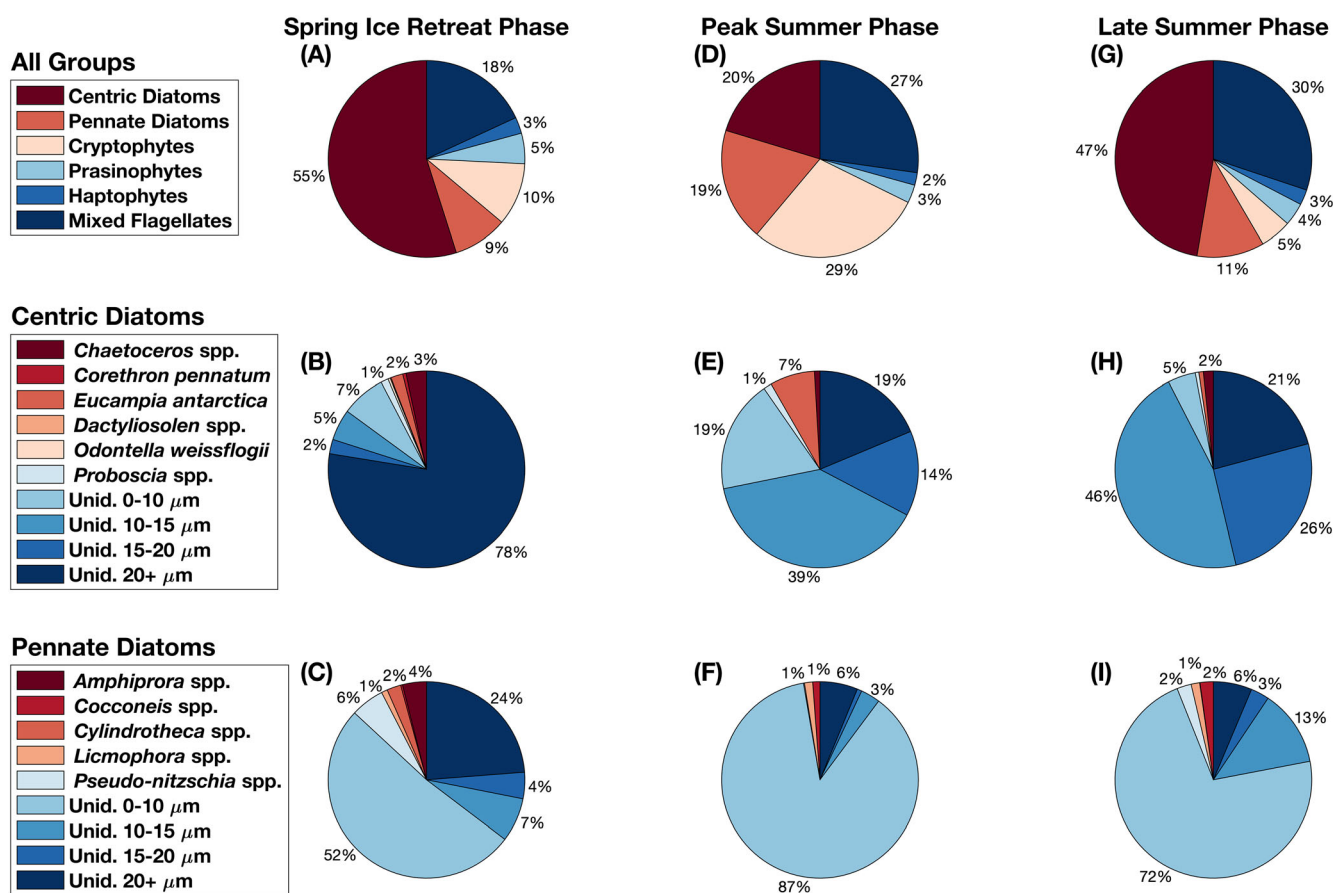


Fig. 6. Percent biovolume for (A, D, G) all taxonomic groups, (B, E, H) centric diatoms and (C, F, I) pennate diatoms during the (A–C) Spring Ice Retreat Phase, (D–F) Peak Summer Phase, and (G–I) Late Summer Phase. Data are aggregated over both years for each phase. The percentage labels for groups with values < 1% were not included. Unid. = Unidentified.

total biovolume), and pennate diatom abundance (19% of total biovolume; Fig. 6D; Table 1). The pennate diatom community was 87% comprised of unidentified cells with diameters < 10 μm (likely including *Fragilariopsis* spp. and *Nitzschia* spp.; Fig. 6F).

The Peak Summer Phase pennate diatom community was especially prevalent in early February 2019 (relative to 2018), when there was a large pennate diatom bloom associated with high water column stability (peak biovolume of $2.43 \mu\text{L L}^{-1}$ on 4 February; Fig. 2). A wind event from 25 January to 28 January (mean 5.34 m s^{-1}) co-occurred with a drop in N^2 , a peak in salinity, a drop in percent meteoric water, and a peak in nutrients (Figs. S5F,H,J,L, S6B,D,F). Just after this wind event, surface PAR increased dramatically and wind speeds dropped, causing percent meteoric water to peak on 04 February corresponding with a dramatic dip in surface temperature, and the lowest salinity, highest N^2 value, highest Chl *a* value, and lowest nutrient concentrations of the field season (Figs. S5B,D,F,H,J,L, S6B,D,F).

The Late Summer Phase was characterized by relatively lower but variable PAR (mean = $282.5 \mu\text{m s}^{-1} \text{ m}^{-1}$), high surface temperatures (mean = 0.9°C), the lowest surface salinities

(mean = 33.1 ppt), highest meteoric water percentages (mean = 5.9%), highest water column stability (mean = 2.0×10^{-4}), low but variable wind speeds (mean = 4.3 m s^{-1}), and low nutrient concentrations (mean nitrate = $21.3 \mu\text{mol L}^{-1}$, mean phosphate = $1.5 \mu\text{mol L}^{-1}$, and mean silicate = $61.9 \mu\text{mol L}^{-1}$; Fig. 5; Table S5). Sea ice concentrations were negligible during this phase (mean = 3.2%; Fig. 5D). The Late Summer Phase was associated with relatively high centric diatom abundance (47% total biovolume) and mixed flagellate abundance (30% total biovolume; Fig. 6G; Table 1). Of the centric diatoms, 46% were unidentified discoid cells with a diameter between 10 and 15 μm and 26% were unidentified discoid cells with a diameter between 15 and 20 μm (likely including smaller *Thalassiosira* spp. and *M. chilensis*; Fig. 6H). Pennate diatom species including *Cocconeis* spp. and *Licmophora* spp. had their highest cell counts during this phase (Table 1).

Matching seasonal succession patterns, phytoplankton median cell size decreased during both field seasons (Figs. 5N, S9). This trend was positively correlated with a decrease in salinity from spring to autumn during both field seasons (Kendall; 2017–2018: $p = 9.45 \times 10^{-4}$ and $\tau = 0.38$; 2018–

2019: $p = 0.04$ and $\tau = 0.22$), suggesting increasing freshwater might be responsible for the decrease in cell size. Surface salinity, percent meteoric water, and upper water-column stability were tightly linked during both years (Fig. 4), with low salinity corresponding to high percent meteoric water (Kendall; 2017–2018: $p = 2.38 \times 10^{-5}$ and $\tau = -0.66$; 2018–2019: $p = 1.88 \times 10^{-5}$ and $\tau = -0.62$) and high N^2 values (Kendall; 2017–2018: $p = 4.61 \times 10^{-12}$ and $\tau = -0.70$; 2018–2019: $p = 2.75 \times 10^{-12}$ and $\tau = -0.67$). Higher N^2 values were also correlated with lower wind speeds (Kendall; 2017–2018: $p = 3.83 \times 10^{-4}$ and $\tau = -0.39$; 2018–2019: $p = 4.93 \times 10^{-6}$ and $\tau = -0.47$), while higher nitrate concentrations were correlated with higher wind speeds (Kendall; 2017–2018: $p = 0.03$ and $\tau = 0.24$; 2018–2019: $p = 0.01$ and $\tau = 0.30$; Fig. 4).

Discussion

This work reveals the mechanisms of winter sea ice dynamics influencing interannual phytoplankton biomass and diatom abundance, as well as the importance of meteoric water in structuring water column stability later in the summer season in tandem with a shift toward smaller phytoplankton cell sizes (e.g., pennate diatoms $< 10 \mu\text{m}$). Despite significant differences in sea ice extent and total phytoplankton biomass between years, phytoplankton successional patterns were remarkably similar and driven by consistent seasonal drivers (e.g., solar irradiance, temperature, and freshwater inputs), while storm/wind events drove more ephemeral differences between years (e.g., the early February 2019 event). Phytoplankton species composition and cell size information collected by the IFCB was invaluable for gaining this more in-depth understanding of seasonal and interannual phytoplankton dynamics at Palmer Station.

Drivers of interannual phytoplankton differences

Along the WAP, phytoplankton demonstrate strong interannual and regional variability, seasonally timed with light availability and spring sea ice retreat. As day length increases in austral spring, solar warming and sea ice melt help to stabilize the upper water column allowing phytoplankton to remain near the surface in waters with higher light availability (Vernet et al. 2008; Venables et al. 2013). These conditions initiate large diatom-dominated spring blooms (Mitchell and Holm-Hansen 1991; Prézelin et al. 2000) as we saw in both field seasons. Similar to other studies, we found that both longer winter sea ice durations (Saba et al. 2014; Rozema et al. 2017; Schofield et al. 2017) and a slower rate of ice-edge retreat in spring to early summer (Garibotti et al. 2005a; Annett et al. 2010; Gonçalves-Araujo et al. 2015) contributed to high phytoplankton abundance and a diatom-dominated community.

Winter sea ice duration was 40 d shorter in 2017 than in 2018, and the phytoplankton community had less diatoms and more mixed flagellates. Wind speed and direction in early

spring (September–October) can precondition the water column due to its effect on sea ice and consequently percent sea ice melt, which in turn could either serve to enhance (as in 2018–2019) or dampen (2017–2018) surface freshening and stratification, influencing phytoplankton biomass and species composition. Although the spring ice-edge retreated later in 2018–2019 than in 2017–2018 (26 December vs. 03 December), the initial phytoplankton bloom occurred earlier due to relatively low ($\sim 30\%$) sea ice coverage starting in early November, allowing adequate light for phytoplankton growth. Sea ice then slowly melted through mid-January, further enhancing surface stratification and stabilizing the upper water column, conditions optimal for phytoplankton growth that in turn contributed to significantly higher Chl *a* concentrations in 2018–2019 (Rozema et al. 2017). In contrast, in 2017, there was $> 50\%$ sea ice coverage through most of November, likely inhibiting light penetration and subsequent phytoplankton growth. Dramatic reduction in sea ice coverage at the end of November indicates rapid, wind-driven advection of sea ice from the region, leading to negative sea ice melt percentages near Palmer Station and allowing high variability in N^2 , likely contributing to the significantly lower Chl *a* concentrations seen during this field season (Rozema et al. 2017).

It is possible that with rapid wind-driven advection of sea ice from the region in 2017, less sea ice algae were released to seed the coastal region near Palmer Station. This can be compared to 2018 when sea ice lingered and contributed more meltwater and potentially more seed populations, with higher associated Chl *a* concentrations in 2018–2019 than in 2017–2018 (Ackley and Sullivan 1994; van Leeuwe et al. 2018). Earlier sea ice advance in the autumn is expected to entrain higher concentrations of algae, therefore, the 16 d earlier sea ice advance in autumn 2018 might also have contributed to increased phytoplankton concentrations in the 2018–2019 field season (Garrison et al. 1983).

Silicate and nitrate were found at significantly higher concentrations in 2018–2019 than in 2017–2018. Typically, years with reduced sea ice and higher wind-driven mixing lead to higher nutrient injection into surface waters from deeper, nutrient-rich waters (Annett et al. 2010). Following this logic, we would expect to see higher nutrient concentrations in 2017–2018. However, there were faster wind speeds at the start of the growing season in 2018 (Spring Ice Retreat Phase mean = 6.5 m s^{-1}) than in 2017 (Spring Ice Retreat Phase mean = 5.0 m s^{-1}) that could have contributed to higher initial concentrations. In addition, there were much larger nutrient drawdown events by high biomass blooms in 2018–2019 than in 2017–2018 that would be expected to lower seasonal nutrient concentrations, emphasizing that wind-driven mixing must have more than compensated for the larger nutrient drawdown in 2018–2019 (Fig. S5K,L).

Taxonomically, there were proportionally more mixed flagellates and prasinophytes in 2017–2018 and proportionally more diatoms and haptophytes in 2018–2019. Dominance of

diatoms and haptophytes (e.g., *P. antarctica*) has been associated with the marginal sea ice zone (Garibotti et al. 2005a), which could explain why we saw higher proportions of both in 2018–2019. Low light environments (e.g., deep mixed layer depths) have been found to favor mixed flagellates (Schofield et al. 2017; Carvalho et al. 2020), thus a significantly higher proportion of mixed flagellates in 2017–2018 may be related to variable N^2 during that field season. In addition, there was higher overall community diversity in 2017–2018, as large diatom blooms in 2018–2019 were dominated by only a few taxonomic groups. This finding was unexpected, as Lin et al. (2021) found less diverse phytoplankton assemblages associated with higher sea surface temperatures, deeper mixed layers, and low sea ice extent along the WAP. Water column stability was not significantly different between our two study years, so it is possible that analyzing additional years with significantly different physical conditions may elicit the patterns seen by Lin et al. (2021).

Drivers of phytoplankton seasonal succession

Following phytoplankton trends found in previous years near Palmer Station (Garibotti et al. 2005a; Schofield et al. 2017), we confirmed three distinct successional phases in both field seasons despite variability in the environmental drivers: a Spring Ice Retreat Phase dominated by large-celled diatoms, followed by a Peak Summer Phase dominated by cryptophytes, followed by a Late Summer Phase dominated by small-celled diatoms. The phytoplankton growing season is initiated during the Spring Ice Retreat Phase as solar irradiance increases (Venables et al. 2013). Matching our results, van Leeuwe et al. (2022) found two ice-associated phytoplankton phases: an initial phase of flagellates such as *Pyramimonas* spp. and *P. antarctica* caused by seeding during sea ice melt (which we saw in higher relative abundance during the Spring Ice Retreat Phase), followed by an increase in large centric diatoms, such as *Thalassiosira* spp. and *Chaetoceros* spp., which are not present within the sea ice but thrive as the upper water column stratifies providing optimal light conditions. This large, stability-induced spring centric diatom bloom has been seen in other Antarctic studies (Garibotti et al. 2005a,b; Costa et al. 2020, 2021) and Arctic studies (Lafond et al. 2019; Ardyna et al. 2020). Overall growth conditions are maximized in years with protracted sea ice retreat (Annett et al. 2010), when greater local sea ice melt enhances surface stratification and promotes phytoplankton growth, illustrated by higher peak biomass and a greater proportion of large, centric diatoms seen in 2018 compared to 2017.

Because the large diatom bloom during the Spring Ice Retreat Phase reduced nutrient concentrations, the next successional phase (Peak Summer Phase) favors mixotrophic phytoplankton such as cryptophytes (Gast et al. 2014; Trefault et al. 2021), that can both photosynthesize and consume particulate organic matter amassed over earlier bloom phases. Cryptophytes are often found in deeper, low-light conditions

where they can supplement photosynthesis with phagotrophy (Goes et al. 2014). However, we saw an increase in surface water biomass during the Peak Summer Phase when PAR and temperature were high, matching other regional studies (Biggs et al. 2019; Pan et al. 2020). High-light environments could give mixotrophs a competitive advantage over heterotrophs, as they can supplement their carbon supply with photosynthesis (Edwards 2019). In addition, cryptophytes are especially well-adapted to high-light environments due to specialized protective pigments (Mendes et al. 2018a). Contrary to other WAP studies (Moline et al. 2004; Schofield et al. 2017; Mendes et al. 2018a), we did not find significant correlations between cryptophytes and low salinity, macronutrients, or percent meteoric water. Thus, it is likely that biotic successional patterns drove this rise in cryptophytes rather than specific abiotic environmental drivers.

In 2018–2019, the Peak Summer Phase also had a very large, stability-induced pennate diatom bloom, likely comprised of *Fragilariopsis* spp. and *Nitzschia* spp. This bloom had almost twice as much biomass as any other bloom seen over both field seasons, possibly because the wind event that preceded the bloom resuspended iron as well as macronutrients, and because smaller diatoms have both high maximum growth rates and an enhanced ability to accelerate growth rates (Behrenfeld et al. 2021). This bloom of small pennate diatoms also co-occurred with a pulse of meteoric water and increased surface stratification (i.e., very high N^2), which has been observed in other field studies (Beans et al. 2008; Höfer et al. 2019; Pan et al. 2020). An experimental study by Hernando et al. (2015) using phytoplankton from Potter Cove, Antarctica found that low salinity conditions (30 PSU) increased the proportion of small pennate diatoms (~0% on day 4 to ~95% on day 8) and decreased the proportion of large centric diatoms (~90% on day 2 to ~0% on day 7), and hypothesized that this was due to differing osmotic stress tolerances. Meteoric water can also carry micronutrients (Annett et al. 2017) that can influence species selection and growth rates, however, micronutrients were not measured in our study. Thus, the pulse of meteoric water during this bloom could have selected for small pennate diatoms with high growth rates.

During the Late Summer Phase, increases in wind-driven mixing replenished nutrients (including iron) to surface waters and allowed for small diatoms (typically 10–20 μm centric diatoms) to bloom. Previous studies show that iron concentrations are important for shifting phytoplankton composition from a phytoflagellate-dominated community to a diatom-dominated community (Boyd et al. 2000). In the Palmer region, iron supply primarily comes from shallow sediments delivered to surface waters by wind-driven vertical mixing (Sherrell et al. 2018). We did not sample iron in this study, but previously collected seasonal data in the Palmer region showed a six-fold increase from late-January to mid-February with increases in wind speed and a deepened mixed

layer depth (Carvalho et al. 2016), which matches the timing of this phase. The Late Summer Phase is characterized by variable mixed layer depths (as inferred from 25 m-averaged N^2), driven by contrasting increases in wind speed and meteoric water inputs. These variable conditions may limit the duration and magnitude of this small diatom bloom. Instead, higher wind-mixing and decreasing daylength in the late summer could select for species that do well in turbulent, low-light environments, resulting in the increased proportion of mixed flagellates that we found (Schofield et al. 2017; Carvalho et al. 2020).

Over the course of both field seasons, we observed decreasing median cell diameter associated with increasing percent meteoric water and decreasing salinity. Stronger surface stratification due to increased freshwater inputs can reduce nutrients in surface waters, giving an advantage to smaller phytoplankton with high surface-area-to-volume ratios and reduced sinking rates (Li et al. 2009). However, macronutrients do not appear to be limiting in either field season, and ratios of Si : N > 2 also suggest no significant limitation by iron or other micronutrients (Clarke et al. 2008). As mentioned above, increased meteoric water inputs could cause cell size and composition shifts via differing tolerances to low salinity, especially for diatoms (Hernando et al. 2015), and via micronutrient inputs (Annett et al. 2017). Since diatoms contributed the highest annual percent composition to the population in low (44% in 2017–2018) and high (66% in 2018–2019) Chl *a* years, cell size shifts in diatoms have a large contribution to the decreasing spring to autumn trend seen in overall phytoplankton cell size.

HPLC vs. IFCB-derived abundance and taxonomy

In general, HPLC and IFCB-derived biomass and percent taxa estimates agreed. There were positive, significant correlations between overall biomass for the two methods and for all taxonomic groups except haptophytes. Similar to other WAP studies (Kozłowski et al. 2011), the strongest relationships between HPLC and imaging (e.g., IFCB and microscopy) methods were found for cryptophyte and diatom percent compositions, and weaker relationships were found for prasinophytes and mixed flagellates. Our results showed that HPLC methods underpredicted mixed flagellates relative to IFCB methods, in agreement with Kozłowski et al. (2011), who suggests this is due to misclassifications of other cells within this group during microscopic analysis. Alternatively, some studies (e.g., Garibotti et al. 2003; Mascioni et al. 2021) have found mixotrophic and heterotrophic dinoflagellates in the WAP, which might be undercounted by HPLC because they have relatively less photosynthetic pigments (e.g., January 2018 in Fig. 2). This might be quite important for years with low sea ice and Chl *a* concentrations that have relatively higher dinoflagellate abundance (Schofield et al. 2017), and would suggest that IFCB or microscopy might be more reliable methods for quantifying mixed flagellate abundance.

In our IFCB samples, we excluded all cells with a major axis length less than 20 pixels (5.88 μm) prior to analysis, as these small cells are below the quantifiable limit of detection based on instrument resolution, and thus have a high probability of being misclassified. *P. antarctica* is mostly found in the flagellate stage during summer in the WAP region below 64°S, with cell diameters < 5 μm (Kozłowski et al. 2011; Biggs et al. 2019). Since *P. antarctica* is the dominant haptophyte in our region (Annett et al. 2010), IFCB methods likely underestimated haptophyte abundances with the exclusion of cells < 5.88 μm , leading to the nonsignificant relationship found between IFCB and HPLC-estimated haptophyte percent composition. This also could be the reason for the slight overprediction of prasinophytes using HPLC compared to IFCB, and thus the weaker correlation between the two methods (Garibotti et al. 2003).

There were a few notable discrepancies in overall abundance between the two methods, particularly on 19 November 2018 and 21 January 2019, where HPLC showed peaks in Chl *a* that were absent or lessened when portrayed by IFCB biovolume. This discrepancy may not be an error in methodology and could instead reflect high Chl *a* to biovolume ratios during these 2 d. However, a potential source of error could be classification within “detritus” and “multiple” categories. Phytoplankton cells were commonly seen attached to detritus particles, or in large conglomerations. These images were eliminated from the analysis as they could not be reliably sorted into a single taxonomic group. Although it is possible that excluding these groups reduced the biovolume in some samples, this does not seem to be the case for the days in question, as total biovolume including non-phytoplankton particles was still very low (see fig. 2 in Nardelli et al. 2022). Although both peaks were dominated by centric diatoms which typically have diameters > 10 μm in this region (Annett et al. 2010), there are some species with diameters < 5.88 μm (e.g., *M. chilensis*), therefore the size cut-off could be responsible for this difference between methods. The absent 21 January 2019 peak could also be the result of preservation bias in the IFCB analysis, as preserved samples were found to have 48% less biovolume than live samples. While some of these discrepancies are errors, some highlight the strength of using these methods in conjunction: HPLC reliably integrates pigments from the whole community regardless of cell size, while automated microscopy can add discriminative ability and information on nonpigmented cells.

Conclusions

This study is one of the first to use both HPLC and an imaging flow cytometer to examine WAP phytoplankton community seasonal succession. While this study contrasts low vs. high Chl *a* years, it is important to note that the succession pattern described in this study is a local phenomenon derived from two seasons. Other studies at Palmer Station (Moline et al. 2004; Schofield et al. 2017), along the PAL-LTER cruise

grid (Garibotti et al. 2005a), in the northern WAP (Varela et al. 2002; Mendes et al. 2013; Trefault et al. 2021), and in the southern WAP (van Leeuwe et al. 2020) found similar succession patterns to ours. However, some areas in the southern WAP (Annett et al. 2010; Rozema et al. 2017; van Leeuwe et al. 2020) and further offshore (Varela et al. 2002), found large *P. antarctica* blooms in the early spring associated with well-mixed water columns and low irradiance. Although we did encounter higher *P. antarctica* abundance in the Spring Ice Retreat Phase, it is possible that we missed a larger early spring bloom by sampling close to shore where sea ice clears out last. High sea ice concentrations inshore might also explain why we saw a large-celled diatom bloom during spring ice retreat in both seasons when other studies sometimes miss this phase (Rozema et al. 2017).

Although this successional pattern is widespread across the WAP, local physical phenomena are important in shaping bloom dynamics. The Palmer Deep Canyon, just offshore from Palmer Station, funnels water counterclockwise around Anvers Island. The residence times of water masses in the canyon are correlated to wind speed, and are on average 2 d with outliers up to 7 d (Kohut et al. 2018), so canyon blooms are somewhat ephemeral and sourced from areas north of Palmer Station. Sta. B is inshore of the canyon and protected by islands, so water mass residence times are likely on the higher end of this spectrum. However, strong wind events can completely reset the system, as evidenced by the large pennate diatom bloom in February 2019. Local phenomena across the WAP can also drive episodic events that do not fit typical succession patterns, such as the massive, nearly monospecific *Pyramimonas* spp. bloom in the Gerlache Strait in January 1987 (Bird and Karl 1991) or the dinoflagellate bloom near Danco Island in December 2016 (Mascioni et al. 2019).

Despite significantly different sea ice conditions and phytoplankton biomass between these 2 yr, phytoplankton biomass began to increase when local sea ice concentration dropped below ~ 50%. The tight coupling between spring sea ice retreat and the start of the phytoplankton growing season leaves this ecosystem vulnerable to phenology shifts induced by climate change. From 1992 to 2015, spring sea ice retreat near Palmer Station shifted earlier by 1.28 d per year (Schofield et al. 2017), and this trend is expected to continue. Earlier sea ice retreat and subsequent water column stratification could shift the start of the growing season earlier: Henson et al. (2018) found that the Southern Ocean spring bloom advances by ~ 5–10 d per decade, which would result in a ~ 50–100 d advance by 2100. This could lead to a mismatch between the timing of the spring bloom and optimal seasonal light levels, and to predator–prey mismatches where spring predators are unable to alter their phenology to match the changes in interannual spring phytoplankton bloom timing (Cushing 1990; Edwards and Richardson 2004; Ardyna et al. 2014).

In addition, our results suggest that protracted sea ice melt in the coastal region could be important for both algal

seeding and promoting phytoplankton growth via increased stratification and light availability, leading to high Chl *a* years dominated by diatoms. Increases in the positive phase of the Southern Annular Mode during austral summer (Thompson and Solomon 2002) cause a higher frequency of strong wind events along the WAP, which could lead to more years like 2017 with rapid sea ice advection from the coastal region. The phytoplankton community seen in 2017–2018 may be representative of future conditions without local sea ice melt, either because high intensity wind events clear the sea ice before local melting can occur, or if there is eventually no persistent winter sea ice. Lin et al. (2021) also found significantly lower species diversity during low sea ice years with high surface temperatures and deep mixed layers. Although we saw higher species diversity during 2017–2018 following a shorter sea ice season, N^2 values were similar between years. Thus, future WAP warming and sea ice loss could cause years with significantly deeper mixed layers than our two study years, and could lead to a decline in phytoplankton species diversity as indicated by Lin et al. (2021).

The use of an IFCB presents a significant observational advantage over HPLC for understanding WAP phytoplankton community dynamics by incorporating both cell size and species information. Higher resolution community composition can help contextualize carbon export, regional biogeochemical cycles, and implications for the broader ecosystem. A shift to smaller phytoplankton species (e.g., through meteoric water increases) reduces carbon export to depth, leading to a microbial-based food web (Ducklow et al. 2013; Sailley et al. 2013). Krill are unable to capture particles < 10 μm due to the filter size of their feeding apparatus (McClatchie and Boyd 1983), whereas microzooplankton selectively feed on smaller phytoplankton (Garzio et al. 2013). In fact, other studies have found a predominance of microzooplankton in coastal waters near glaciers with high proportions of small phytoplankton cells (Beans et al. 2008; Garcia et al. 2019). Thus, a shift to smaller phytoplankton cells could lengthen the food web by adding an intermediate microzooplankton step between phytoplankton and krill, reducing trophic efficiency (Bernard et al. 2012) and krill lipid content (Ruck et al. 2014), and in turn negatively impacting top predator populations. Given the taxonomic resolution from HPLC measurements, these size and species level community dynamics would be missed. Thus, continuation of seasonal phytoplankton size and species measurements using tools like the IFCB will be important to understand the impacts of environmental change along the WAP.

Data availability statement

HPLC, macronutrient, wind speed, and PAR data are available at <https://pallter.marine.rutgers.edu/data>. CTD, IFCB, sea ice, and $\delta^{18}\text{O}$ data will be shared on reasonable request to the corresponding author.

References

- Ackley, S. F., and C. W. Sullivan. 1994. Physical controls on the development and characteristics of Antarctic Sea ice biological communities—A review and synthesis. *Deep-Sea Res. I: Oceanogr. Res. Pap.* **41**: 1583–1604. doi:[10.1016/0967-0637\(94\)90062-0](https://doi.org/10.1016/0967-0637(94)90062-0)
- Annett, A. L., D. S. Carson, X. Crosta, A. Clarke, and R. S. Ganeshram. 2010. Seasonal progression of diatom assemblages in surface waters of Ryder Bay, Antarctica. *Polar Biol.* **33**: 13–29. doi:[10.1007/s00300-009-0681-7](https://doi.org/10.1007/s00300-009-0681-7)
- Annett, A. L., J. N. Fitzsimmons, M. J. M. Séguret, M. Lagerstrom, M. P. Meredith, O. Schofield, and R. M. Sherrell. 2017. Controls on dissolved and particulate iron distributions in surface waters of the Western Antarctic Peninsula shelf. *Mar. Chem.* **196**: 81–97. doi:[10.1016/j.marchem.2017.06.004](https://doi.org/10.1016/j.marchem.2017.06.004)
- Ardyna, M., M. Babin, M. Gosselin, E. Devred, L. Rainville, and J.-É. Tremblay. 2014. Recent Arctic Ocean sea ice loss triggers novel fall phytoplankton blooms. *Geophys. Res. Lett.* **41**: 6207–6212. doi:[10.1002/2014GL061047](https://doi.org/10.1002/2014GL061047)
- Ardyna, M., and others. 2020. Environmental drivers of under-ice phytoplankton bloom dynamics in the Arctic Ocean. *Elementa* **8**: 30. doi:[10.1525/elementa.430](https://doi.org/10.1525/elementa.430)
- Arrigo, K. R., G. L. van Dijken, and S. Bushinsky. 2008. Primary production in the Southern Ocean, 1997–2006. *J. Geophys. Res.* **113**: C08004. doi:[10.1029/2007JC004551](https://doi.org/10.1029/2007JC004551)
- Beans, C., J. H. Hecq, P. Koubbi, C. Vallet, S. Wright, and A. Goffart. 2008. A study of the diatom-dominated microplankton summer assemblages in coastal waters from Terre Adélie to the Mertz Glacier, East Antarctica (139°E–145°E). *Polar Biol.* **31**: 1101–1117. doi:[10.1007/s00300-008-0452-x](https://doi.org/10.1007/s00300-008-0452-x)
- Behrenfeld, M. J., K. H. Halsey, E. Boss, L. Karp-Boss, A. J. Milligan, and G. Peers. 2021. Thoughts on the evolution and ecological niche of diatoms. *Ecol. Monogr.* **91**: e01457. doi:[10.1002/ecm.1457](https://doi.org/10.1002/ecm.1457)
- Bernard, K. S., D. K. Steinberg, and O. M. E. Schofield. 2012. Summertime grazing impact of the dominant macrozooplankton off the Western Antarctic Peninsula. *Deep-Sea Res. I: Oceanogr. Res. Pap.* **62**: 111–122. doi:[10.1016/j.dsr.2011.12.015](https://doi.org/10.1016/j.dsr.2011.12.015)
- Biggs, T. E. G., S. Alvarez-Fernandez, C. Evans, K. D. A. Mojica, P. D. Rozema, H. J. Venables, D. W. Pond, and C. P. D. Brussaard. 2019. Antarctic phytoplankton community composition and size structure: Importance of ice type and temperature as regulatory factors. *Polar Biol.* **42**: 1997–2015. doi:[10.1007/s00300-019-02576-3](https://doi.org/10.1007/s00300-019-02576-3)
- Bird, D. F., and D. M. Karl. 1991. Massive prasinophyte bloom in northern Gerlache Strait. *Antarct. J.* **26**: 152–154.
- Boyd, P. W., and others. 2000. A mesoscale phytoplankton bloom in the polar Southern Ocean stimulated by iron fertilization. *Nature* **407**: 695–702. doi:[10.1038/35037500](https://doi.org/10.1038/35037500)
- Carvalho, F., J. Kohut, M. J. Oliver, R. M. Sherrell, and O. Schofield. 2016. Mixing and phytoplankton dynamics in a submarine canyon in the West Antarctic Peninsula. *J. Geophys. Res.: Oceans* **121**: 5069–5083. doi:[10.1002/2016JC011650](https://doi.org/10.1002/2016JC011650)
- Carvalho, F., J. Kohut, M. J. Oliver, and O. Schofield. 2017. Defining the ecologically relevant mixed-layer depth for Antarctica's coastal seas. *Geophys. Res. Lett.* **44**: 338–345. doi:[10.1002/2016GL071205](https://doi.org/10.1002/2016GL071205)
- Carvalho, F., and others. 2020. Testing the canyon hypothesis: Evaluating light and nutrient controls of phytoplankton growth in penguin foraging hotspots along the West Antarctic Peninsula. *Limnol. Oceanogr.* **65**: 455–470. doi:[10.1002/lno.11313](https://doi.org/10.1002/lno.11313)
- Clarke, A., M. P. Meredith, M. I. Wallace, M. A. Brandon, and D. N. Thomas. 2008. Seasonal and interannual variability in temperature, chlorophyll and macronutrients in northern Marguerite Bay, Antarctica. *Deep-Sea Res. II: Top. Stud. Oceanogr.* **55**: 1988–2006. doi:[10.1016/j.dsr2.2008.04.035](https://doi.org/10.1016/j.dsr2.2008.04.035)
- Cook, A. J., P. R. Holland, M. P. Meredith, T. Murray, A. Luckman, and D. G. Vaughan. 2016. Ocean forcing of glacier retreat in the western Antarctic Peninsula. *Science* **353**: 283–286. doi:[10.1126/science.aae0017](https://doi.org/10.1126/science.aae0017)
- Costa, R. R., C. R. B. Mendes, V. M. Tavano, T. S. Dotto, R. Kerr, T. Monteiro, C. Odebrecht, and E. R. Secchi. 2020. Dynamics of an intense diatom bloom in the Northern Antarctic Peninsula, February 2016. *Limnol. Oceanogr.* **65**: 2056–2075. doi:[10.1002/lno.11437](https://doi.org/10.1002/lno.11437)
- Costa, R. R., C. R. B. Mendes, A. Ferreira, V. M. Tavano, T. S. Dotto, and E. R. Secchi. 2021. Large diatom bloom off the Antarctic peninsula during cool conditions associated with the 2015/2016 El Niño. *Commun. Earth Environ.* **2**: 252. doi:[10.1038/s43247-021-00322-4](https://doi.org/10.1038/s43247-021-00322-4)
- Cushing, D. H. 1990. Plankton production and year-class strength in fish populations: An update of the match/mismatch hypothesis, p. 249–293. *In* J. H. S. Blaxter and A. J. Southward [eds.], *Advances in marine biology*, v. **26**. Elsevier. doi:[10.1016/S0065-2881\(08\)60202-3](https://doi.org/10.1016/S0065-2881(08)60202-3)
- Ducklow, H. W., and others. 2013. West Antarctic Peninsula: An ice-dependent coastal marine ecosystem in transition. *Oceanography* **26**: 190–203. doi:[10.5670/oceanog.2013.62](https://doi.org/10.5670/oceanog.2013.62)
- Edwards, K. F. 2019. Mixotrophy in nanoflagellates across environmental gradients in the ocean. *Proc. Natl. Acad. Sci. USA* **116**: 6211–6220. doi:[10.1073/pnas.1814860116](https://doi.org/10.1073/pnas.1814860116)
- Edwards, M., and A. J. Richardson. 2004. Impact of climate change on marine pelagic phenology and trophic mismatch. *Nature* **430**: 881–884. doi:[10.1038/nature02808](https://doi.org/10.1038/nature02808)
- Garcia, M. D., and others. 2019. Effects of glacier melting on the planktonic communities of two Antarctic coastal areas (Potter Cove and Hope Bay) in summer. *Reg. Stud. Mar. Sci.* **30**: 100731. doi:[10.1016/j.rsma.2019.100731](https://doi.org/10.1016/j.rsma.2019.100731)
- Garibotti, I. A., M. Vernet, W. A. Kozłowski, and M. E. Ferrario. 2003. Composition and biomass of phytoplankton assemblages in coastal Antarctic waters: A comparison of chemotaxonomic and microscopic analyses. *Mar. Ecol. Prog. Ser.* **247**: 27–42. doi:[10.3354/meps247027](https://doi.org/10.3354/meps247027)

- Garibotti, I. A., M. Vernet, and M. E. Ferrario. 2005a. Annually recurrent phytoplanktonic assemblages during summer in the seasonal ice zone west of the Antarctic Peninsula (Southern Ocean). *Deep-Sea Res. I: Oceanogr. Res. Pap.* **52**: 1823–1841. doi:10.1016/j.dsr.2005.05.003
- Garibotti, I. A., M. Vernet, R. C. Smith, and M. E. Ferrario. 2005b. Interannual variability in the distribution of the phytoplankton standing stock across the seasonal sea-ice zone west of the Antarctic Peninsula. *J. Plankton Res.* **27**: 825–843. doi:10.1093/plankt/fbi056
- Garrison, D. L., S. F. Ackley, and K. R. Buck. 1983. A physical mechanism for establishing algal populations in frazil ice. *Nature* **306**: 363–365. doi:10.1038/306363a0
- Garzio, L. M., D. K. Steinberg, M. Erickson, and H. W. Ducklow. 2013. Microzooplankton grazing along the Western Antarctic Peninsula. *Aquat. Microb. Ecol.* **70**: 215–232. doi:10.3354/ame01655
- Gast, R. J., Z. M. McKie-Krisberg, S. A. Fay, J. M. Rose, and R. W. Sanders. 2014. Antarctic mixotrophic protist abundances by microscopy and molecular methods. *FEMS Microbiol. Ecol.* **89**: 388–401. doi:10.1111/1574-6941.12334
- Goes, J. I., and others. 2014. Influence of the Amazon River discharge on the biogeography of phytoplankton communities in the western tropical North Atlantic. *Prog. Oceanogr.* **120**: 29–40. doi:10.1016/j.pocean.2013.07.010
- Gonçalves-Araujo, R., M. S. de Souza, V. M. Tavano, and C. A. E. Garcia. 2015. Influence of oceanographic features on spatial and interannual variability of phytoplankton in the Bransfield Strait, Antarctica. *J. Mar. Syst.* **142**: 1–15. doi:10.1016/j.jmarsys.2014.09.007
- Hasle, G. R., E. E. Syvertsen, K. A. Steidinger, K. Tangen, J. Thronsen, and B. R. Heimdal. 1997. In C. R. Tomas [ed.], *Identifying marine phytoplankton*. Academic Press.
- Henson, S. A., H. S. Cole, J. Hopkins, A. P. Martin, and A. Yool. 2018. Detection of climate change-driven trends in phytoplankton phenology. *Glob. Change Biol.* **24**: e101–e111. doi:10.1111/gcb.13886
- Hernando, M., I. R. Schloss, G. Malanga, G. O. Almandoz, G. A. Ferreyra, M. B. Aguiar, and S. Puntarulo. 2015. Effects of salinity changes on coastal Antarctic phytoplankton physiology and assemblage composition. *J. Exp. Mar. Bio. Ecol.* **466**: 110–119. doi:10.1016/j.jembe.2015.02.012
- Höfer, J., R. Giesecke, M. J. Hopwood, V. Carrera, E. Alarcón, and H. E. González. 2019. The role of water column stability and wind mixing in the production/export dynamics of two bays in the Western Antarctic peninsula. *Prog. Oceanogr.* **174**: 105–116. doi:10.1016/j.pocean.2019.01.005
- Kaňa, R., E. Kotabová, R. Sobotka, and O. Prášil. 2012. Non-photochemical quenching in cryptophyte alga *Rhodomonas salina* is located in chlorophyll a/c antennae. *PLoS One* **7**: e29700. doi:10.1371/journal.pone.0029700
- Kim, H., S. C. Doney, R. A. Iannuzzi, M. P. Meredith, D. G. Martinson, and H. W. Ducklow. 2016. Climate forcing for dynamics of dissolved inorganic nutrients at Palmer Station, Antarctica: An interdecadal (1993–2013) analysis. *J. Geophys. Res.: Biogeosciences* **121**: 2369–2389. doi:10.1002/2015JG003311
- Kim, H., and others. 2018. Inter-decadal variability of phytoplankton biomass along the coastal West Antarctic Peninsula. *Philos. Trans. R. Soc. A* **376**: 20170174. doi:10.1098/rsta.2017.0174
- Kohut, J. T., P. Winsor, H. Statscewich, M. J. Oliver, E. Fredj, N. Couto, K. Bernard, and W. Fraser. 2018. Variability in summer surface residence time within a West Antarctic Peninsula biological hotspot. *Philos. Trans. R. Soc. A* **376**: 20170165. doi:10.1098/rsta.2017.0165
- Kozłowski, W. A., D. Deutschman, I. Garibotti, C. Trees, and M. Vernet. 2011. An evaluation of the application of CHEMTAX to Antarctic coastal pigment data. *Deep-Sea Res. I: Oceanogr. Res. Pap.* **58**: 350–364. doi:10.1016/j.dsr.2011.01.008
- Lafond, A., and others. 2019. Late spring bloom development of pelagic diatoms in Baffin Bay. *Elementa* **7**: 44. doi:10.1525/elementa.382
- Li, W. K. W., F. A. McLaughlin, C. Lovejoy, and E. C. Carmack. 2009. Smallest algae thrive as the Arctic Ocean freshens. *Science* **326**: 539. doi:10.1126/science.1179798
- Lin, Y., and others. 2021. Decline in plankton diversity and carbon flux with reduced sea ice extent along the Western Antarctic Peninsula. *Nat. Commun.* **12**: 4948. doi:10.1038/s41467-021-25235-w
- Lorbacher, K., D. Dommenges, P. P. Niiler, and A. Köhl. 2006. Ocean mixed layer depth: A subsurface proxy of ocean-atmosphere variability. *J. Geophys. Res.* **111**: C07010. doi:10.1029/2003JC002157
- Mascioni, M., G. O. Almandoz, A. O. Cefarelli, A. Cusick, M. E. Ferrario, and M. Vernet. 2019. Phytoplankton composition and bloom formation in unexplored nearshore waters of the Western Antarctic Peninsula. *Polar Biol.* **42**: 1859–1872. doi:10.1007/s00300-019-02564-7
- Mascioni, M., G. O. Almandoz, L. Ekern, B. J. Pan, and M. Vernet. 2021. Microplanktonic diatom assemblages dominated the primary production but not the biomass in an Antarctic fjord. *J. Mar. Syst.* **224**: 103624. doi:10.1016/j.jmarsys.2021.103624
- McClatchie, S., and C. M. Boyd. 1983. Morphological study of sieve efficiencies and mandibular surfaces in the Antarctic Krill, *Euphausia superba*. *Can. J. Fish. Aquat. Sci.* **40**: 955–967. doi:10.1139/f83-122
- Mendes, C. R. B., V. M. Tavano, M. C. Leal, M. S. de Souza, V. Brotas, and C. A. E. Garcia. 2013. Shifts in the dominance between diatoms and cryptophytes during three late summers in the Bransfield Strait (Antarctic Peninsula). *Polar Biol.* **36**: 537–547. doi:10.1007/s00300-012-1282-4
- Mendes, C. R. B., V. M. Tavano, T. S. Dotto, R. Kerr, M. S. de Souza, C. A. E. Garcia, and E. R. Secchi. 2018a. New

- insights on the dominance of cryptophytes in Antarctic coastal waters: A case study in Gerlache Strait. *Deep-Sea Res. II: Top. Stud. Oceanogr.* **149**: 161–170. doi:[10.1016/j.dsr2.2017.02.010](https://doi.org/10.1016/j.dsr2.2017.02.010)
- Mendes, C. R. B., V. M. Tavano, R. Kerr, T. S. Dotto, T. Maximiano, and E. R. Secchi. 2018b. Impact of sea ice on the structure of phytoplankton communities in the northern Antarctic Peninsula. *Deep-Sea Res. II: Top. Stud. Oceanogr.* **149**: 111–123. doi:[10.1016/j.dsr2.2017.12.003](https://doi.org/10.1016/j.dsr2.2017.12.003)
- Meredith, M. P., and J. C. King. 2005. Rapid climate change in the ocean west of the Antarctic Peninsula during the second half of the 20th century. *Geophys. Res. Lett.* **32**: L19604. doi:[10.1029/2005GL024042](https://doi.org/10.1029/2005GL024042)
- Meredith, M. P., H. J. Venables, A. Clarke, H. W. Ducklow, M. Erickson, M. J. Leng, J. T. M. Lenaerts, and M. R. van den Broeke. 2013. The freshwater system west of the Antarctic Peninsula: Spatial and temporal changes. *J. Climate* **26**: 1669–1684. doi:[10.1175/JCLI-D-12-00246.1](https://doi.org/10.1175/JCLI-D-12-00246.1)
- Meredith, M. P., and others. 2017. Changing distributions of sea ice melt and meteoric water west of the Antarctic Peninsula. *Deep-Sea Res. II: Top. Stud. Oceanogr.* **139**: 40–57. doi:[10.1016/j.dsr2.2016.04.019](https://doi.org/10.1016/j.dsr2.2016.04.019)
- Meredith, M. P., and others. 2021. Local- and large-scale drivers of variability in the coastal freshwater budget of the Western Antarctic Peninsula. *J. Geophys. Res.: Oceans* **126**: e2021JC017172. doi:[10.1029/2021JC017172](https://doi.org/10.1029/2021JC017172)
- Mitchell, B. G., and O. Holm-Hansen. 1991. Bio-optical properties of Antarctic Peninsula waters: Differentiation from temperate ocean models. *Deep-Sea Res. I: Oceanogr. Res. Pap.* **38**: 1009–1028. doi:[10.1016/0198-0149\(91\)90094-V](https://doi.org/10.1016/0198-0149(91)90094-V)
- Moline, M. A., H. Claustre, T. K. Frazer, O. Schofield, and M. Vernet. 2004. Alteration of the food web along the Antarctic Peninsula in response to a regional warming trend. *Glob. Change Biol.* **10**: 1973–1980. doi:[10.1111/j.1365-2486.2004.00825.x](https://doi.org/10.1111/j.1365-2486.2004.00825.x)
- Montes-Hugo, M., S. C. Doney, H. W. Ducklow, W. Fraser, D. Martinson, S. E. Stammerjohn, and O. Schofield. 2009. Recent changes in phytoplankton communities associated with rapid regional climate change along the Western Antarctic Peninsula. *Science* **323**: 1470–1473. doi:[10.1126/science.1164533](https://doi.org/10.1126/science.1164533)
- Nardelli, S. C., P. C. Gray, and O. Schofield. 2022. A convolutional neural network to classify phytoplankton images along the West Antarctic Peninsula. *Mar. Technol. Soc. J.* **56**: 45–57. doi:[10.4031/MTSJ.56.5.8](https://doi.org/10.4031/MTSJ.56.5.8)
- Olson, R. J., and H. M. Sosik. 2007. A submersible imaging-inflow instrument to analyze nano-and microplankton: Imaging FlowCytobot. *Limnol. Oceanogr.: Methods* **5**: 195–203. doi:[10.4319/lom.2007.5.195](https://doi.org/10.4319/lom.2007.5.195)
- Pan, B. J., and others. 2020. Environmental drivers of phytoplankton taxonomic composition in an Antarctic fjord. *Prog. Oceanogr.* **183**: 102295. doi:[10.1016/j.pocean.2020.102295](https://doi.org/10.1016/j.pocean.2020.102295)
- Picheral, M., C. E. Sanders, and J.-O. Irisson. 2017. EcoTaxa, a tool for the taxonomic classification of images. <http://ecotaxa.obs-vlfr.fr>
- Prézelin, B. B., E. E. Hofmann, C. Mengelt, and J. M. Klinck. 2000. The linkage between Upper Circumpolar Deep Water (UCDW) and phytoplankton assemblages on the West Antarctic Peninsula continental shelf. *J. Mar. Res.* **58**: 165–202. doi:[10.1357/002224000321511133](https://doi.org/10.1357/002224000321511133)
- Rozema, P. D., H. J. Venables, W. H. van de Poll, A. Clarke, M. P. Meredith, and A. G. J. Buma. 2017. Interannual variability in phytoplankton biomass and species composition in northern Marguerite Bay (West Antarctic Peninsula) is governed by both winter sea ice cover and summer stratification. *Limnol. Oceanogr.* **62**: 235–252. doi:[10.1002/lno.10391](https://doi.org/10.1002/lno.10391)
- Ruck, K. E., D. K. Steinberg, and E. A. Canuel. 2014. Regional differences in quality of krill and fish as prey along the Western Antarctic Peninsula. *Mar. Ecol. Prog. Ser.* **509**: 39–55. doi:[10.3354/meps10868](https://doi.org/10.3354/meps10868)
- Saba, G. K., and others. 2014. Winter and spring controls on the summer food web of the coastal West Antarctic Peninsula. *Nat. Commun.* **5**: 4318. doi:[10.1038/ncomms5318](https://doi.org/10.1038/ncomms5318)
- Sailley, S. F., H. W. Ducklow, H. V. Moeller, W. R. Fraser, O. M. Schofield, D. K. Steinberg, L. M. Garzio, and S. C. Doney. 2013. Carbon fluxes and pelagic ecosystem dynamics near two western Antarctic Peninsula Adélie penguin colonies: An inverse model approach. *Mar. Ecol. Prog. Ser.* **492**: 253–272. doi:[10.3354/meps10534](https://doi.org/10.3354/meps10534)
- Schofield, O., and others. 2017. Decadal variability in coastal phytoplankton community composition in a changing West Antarctic Peninsula. *Deep-Sea Res. I: Oceanogr. Res. Pap.* **124**: 42–54. doi:[10.1016/j.dsr.2017.04.014](https://doi.org/10.1016/j.dsr.2017.04.014)
- Scott, F. J., and H. J. Marchant [eds.]. 2005. Antarctic marine protists. Australian Biological Resources Study.
- Sherrell, R. M., A. L. Annett, J. N. Fitzsimmons, V. J. Rocanova, and M. P. Meredith. 2018. A ‘shallow bathtub ring’ of local sedimentary iron input maintains the palmer deep biological hotspot on the West Antarctic Peninsula shelf. *Philos. Trans. R. Soc. A* **376**: 20170171. doi:[10.1098/rsta.2017.0171](https://doi.org/10.1098/rsta.2017.0171)
- Sosik, H. M., and R. J. Olson. 2007. Automated taxonomic classification of phytoplankton sampled with imaging-inflow cytometry. *Limnol. Oceanogr.: Methods* **5**: 204–216. doi:[10.4319/lom.2007.5.204](https://doi.org/10.4319/lom.2007.5.204)
- Stammerjohn, S. E., D. G. Martinson, R. C. Smith, X. Yuan, and D. Rind. 2008. Trends in Antarctic annual sea ice retreat and advance and their relation to El Niño–Southern Oscillation and Southern Annular Mode variability. *J. Geophys. Res.: Oceans* **113**: C03S90. doi:[10.1029/2007JC004269](https://doi.org/10.1029/2007JC004269)
- Stammerjohn, S., R. Massom, D. Rind, and D. Martinson. 2012. Regions of rapid sea ice change: An inter-hemispheric seasonal comparison. *Geophys. Res. Lett.* **39**: L06501. doi:[10.1029/2012GL050874](https://doi.org/10.1029/2012GL050874)
- Thompson, D. W. J., and S. Solomon. 2002. Interpretation of recent Southern Hemisphere climate change. *Science* **296**: 895–899. doi:[10.1126/science.1069270](https://doi.org/10.1126/science.1069270)

- Trefault, N., and others. 2021. Annual phytoplankton dynamics in coastal waters from Fildes Bay, Western Antarctic Peninsula. *Sci. Rep.* **11**: 1368. doi:10.1038/s41598-020-80568-8
- Turner, J., and others. 2005. Antarctic climate change during the last 50 years. *Int. J. Climatol.* **25**: 279–294. doi:10.1002/joc.1130
- van Leeuwe, M. A., and others. 2018. Microalgal community structure and primary production in Arctic and Antarctic Sea ice: A synthesis. *Elementa* **6**: 4. doi:10.1525/elementa.267
- van Leeuwe, M. A., A. L. Webb, H. J. Venables, R. J. W. Visser, M. P. Meredith, J. T. M. Elzenga, and J. Stefels. 2020. Annual patterns in phytoplankton phenology in Antarctic coastal waters explained by environmental drivers. *Limnol. Oceanogr.* **65**: 1651–1668. doi:10.1002/lno.11477
- van Leeuwe, M. A., M. Fenton, E. Davey, J. -M. Rintala, E. M. Jones, M. P. Meredith, and J. Stefels. (2022). On the phenology and seeding potential of sea-ice microalgal species. *Elementa: Science of the Anthropocene* **10**(1). doi:10.1525/elementa.2021.00029
- Varela, M., E. Fernandez, and P. Serret. 2002. Size-fractionated phytoplankton biomass and primary production in the Gerlache and south Bransfield Straits (Antarctic Peninsula) in austral summer 1995–1996. *Deep-Sea Res. II: Top. Stud. Oceanogr.* **49**: 749–768. doi:10.1016/S0967-0645(01)00122-9
- Venables, H. J., A. Clarke, and M. P. Meredith. 2013. Winter-time controls on summer stratification and productivity at the Western Antarctic Peninsula. *Limnol. Oceanogr.* **58**: 1035–1047. doi:10.4319/lo.2013.58.3.1035
- Vernet, M., and R. C. Smith. 2007. Measuring and modeling primary production in marine pelagic ecosystems, p. 142–174. *In* T. J. Fahey and A. K. Knapp [eds.], *Principles and standards for measuring primary production*. Oxford Univ. Press.
- Vernet, M., D. Martinson, R. Iannuzzi, S. Stammerjohn, W. Kozlowski, K. Sines, R. Smith, and I. Garibotti. 2008. Primary production within the sea-ice zone west of the Antarctic Peninsula: I—Sea ice, summer mixed layer, and irradiance. *Deep-Sea Res. II: Top. Stud. Oceanogr.* **55**: 2068–2085. doi:10.1016/j.dsr2.2008.05.021

Acknowledgments

This work was supported by the National Science Foundation Antarctic Organisms and Ecosystems Program (PLR-1440435) as part of the PAL-LTER program, and by NASA (19-IDS19-0085). In addition, S.N. acknowledges support from the Rutgers Institute of Earth, Ocean, and Atmospheric Sciences graduate fellowship. HPLC data was provided by Nicole Waite, $\delta^{18}\text{O}$ data for meltwater calculations was provided by Michael Meredith, and nutrient data was provided by Naomi Manahan. Frank McQuarrie, Taylor Dodge, Marie Zahn, Anna Bashkirova, and Hailey Conrad helped with data collection in the field. Thank you to Alison Chase and Sasha Kramer for help with phytoplankton taxonomic identifications. This work would not have been possible without Palmer Station personnel, particularly the marine technicians, lab manager, and instrument technicians from the 2017–2018 and 2018–2019 field seasons. Comments from three anonymous reviewers helped improve and clarify this manuscript.

Conflict of Interest

None declared.

Submitted 09 May 2022

Revised 06 November 2022

Accepted 18 January 2023

Deputy editor: C. Elisa Schaum